Magnetic properties and heat capacity of the three-dimensional frustrated $S = \frac{1}{2}$ antiferromagnet $PbCuTe_2O_6$

B. Koteswararao,[1,2] R. Kumar,[3] P. Khuntia,[4,*] Sayantika Bhowal,[5] S. K. Panda,[6] M. R. Rahman,[1] A. V. Mahajan,[3] I. Dasgupta,[5,6] M. Baenitz,[4] Kee Hoon Kim,[2,†] and F. C. Chou[1,‡]

[1]*Center of Condensed Matter Sciences, National Taiwan University, Taipei 10617, Taiwan*

[2]*CeNSCMR, Department of Physics and Astronomy, and Institute of Applied Physics, Seoul National University, Seoul 151-747, South Korea*

[3]*Department of Physics, Indian Institute of Technology Bombay, Mumbai 400076, India*

[4]*Max Planck Institute for Chemical Physics of Solids, 01187 Dresden, Germany*

[5]*Department of Solid State Physics, Indian Association for the Cultivation of Science, Jadavpur, Kolkata-700032, India*

[6]*Centre for Advanced Materials, Indian Association for the Cultivation of Science, Jadavpur, Kolkata-700032, India*

(Received 22 March 2014; revised manuscript received 27 June 2014; published 29 July 2014)

We report magnetic susceptibility (χ) and heat capacity (C_p) measurements along with *ab initio* electronic structure calculations on $PbCuTe_2O_6$, a compound made up of a three-dimensional (3D) network of corner-shared triangular units. The presence of antiferromagnetic interactions is inferred from a Curie-Weiss temperature (θ_{CW}) of about -22 K from the $\chi(T)$ data. The magnetic heat capacity C_m data show a broad maximum at $T^{max} \simeq 1.15$ K (i.e., $T^{max}/\theta_{CW} \simeq 0.05$), which is analogous to the the observed broad maximum in the C_m/T data of a hyper-kagome system, $Na_4Ir_3O_8$. In addition, C_m data exhibit a weak kink at $T^* \simeq 0.87$ K. While the T^{max} is nearly unchanged, the T^* is systematically suppressed in an increasing magnetic field (H) up to 80 kOe. For $H \geqslant 80$ kOe, the C_m data at low temperatures exhibit a characteristic power-law (T^α) behavior with an exponent α slightly less than 2. Hopping integrals obtained from the electronic structure calculations show the presence of strongly frustrated 3D spin interactions along with non-negligible unfrustrated couplings. Our results suggest that $PbCuTe_2O_6$ is a candidate material for realizing a 3D quantum spin liquid state at high magnetic fields.

DOI: 10.1103/PhysRevB.90.035141 PACS number(s): 75.40.Cx, 75.10.Kt

I. INTRODUCTION

Interesting magnetic behavior in Heisenberg spin systems originates from a network of some elementary motifs such as triangles or tetrahedra, where the spins placed at their vertices interact with each other via antiferromagnetic interactions. Due to the incompatibility of the nearest-neighbor interactions of a spin with respect to achieving the lowest energy, these systems ideally do not have any conventional, symmetry-breaking, phase transition. Instead, they often lead to exotic ground states such as spin liquids and spin ice states [1–3]. There are many well-known experimental examples for the three-dimensional (3D) networks of corner-shared tetrahedra, particularly in the pyrochlore and spinel structures [3]. On the other hand, 3D networks of corner-shared triangles are relatively less explored, despite the expectation that they would also display novel ground states.

Two representative systems in the family of 3D corner-shared triangles are $Gd_3Ga_5O_{12}$ [4–6] and $Na_4Ir_3O_8$ [7]. The $Gd_3Ga_5O_{12}$ compound comprises of two interpenetrating hyper-kagome networks, in which 3D coupled, corner-shared triangles of Gd^{3+} ($4f^7$ with $S = 7/2$) spins are realized with coordination number $z = 4$ as in the case of the two-dimensional (2D) kagome networks. The Gd system does not order down to 25 mK in spite of a relatively large Curie-Weiss temperature (θ_{CW}) of -2.3 K [4], indicating that it is highly frustrated. It has a rich magnetic phase diagram as investigated by magnetic susceptibility, heat capacity [5], and inelastic neutron scattering (INS) experiments [6]. $Na_4Ir_3O_8$ forms a perfect hyper-kagome network composed of $5d$ Ir^{4+} ions, and is considered as the first example of a 3D, $J_{eff} = 1/2$ frustrated antiferromagnet with a quantum spin liquid (QSL) ground state. The $5d$-based transition-metal oxides are known for having a large spin-orbit coupling and yet the $Na_4Ir_3O_8$ system retains the spin liquid ground state [8]. The exchange coupling between Ir^{4+} spins is estimated to be about $J/k_B \simeq -300$ K and the θ_{CW} is about -650 K, while no signature of ordering is found down to 2 K. Many theoretical studies have also suggested that $Na_4Ir_3O_8$ is a promising candidate for the 3D QSL ground state [9].

As far as the 3d transition-metal based oxides are concerned, the spin liquid state has been more widely found in the 2D corner- and edge-shared frustrated triangular systems; $S = 1/2$ Cu^{2+}-based kagome lattices $ZnCu_3(OH)_6Cl_2$ (herberthsmithite [10] and kapellasite [11]), $S = 1/2$ V^{4+}-based 2D kagome lattice $[NH_4]_2[C_7H_{14}N][V_7O_6F_{18}]$ [12], $S = 1/2$ triangular lattices κ-$(ET)_2Cu_2(CN)_3$ [13], and $Ba_3CuSb_2O_9$ [14,15]. To our knowledge, however, a candidate for the $S = 1/2$, 3D QSL ground state in the 3d transition-metal oxides has not been reported so far.

Herein, we introduce a new candidate with a Cu-based 3D network, $PbCuTe_2O_6$, which is isostructural to a mineral compound choloalite $PbCuTe_2O_6Cl_{0.333}$ [16]. The compound crystallizes in a cubic structure with the space-group $P4_132$ (No. 213) and has a 3D network of Cu atoms, where the first nearest neighbors (nn) form uniform triangles, the second nn form a hyper-kagome network and the third nn form uniform chains running in all the crystallographic directions. The magnetic susceptibility $\chi(T)$ reveals a Curie-Weiss behavior ($\theta_{CW} \simeq -22$ K) down to 2 K with no bifurcation between

*Present address: The Ames Laboratory, US Department of Energy, Ames, IA 50011, USA.

†khkim@phya.snu.ac.kr

‡fcchou@ntu.edu.tw

zero-field-cooled (ZFC) and field-cooled (FC) curves at low fields. However, the heat capacity $C_p(T)$ data at zero magnetic field show a broad maximum at $T^{\max} \simeq 1.15$ K and also a weak kink, at $T^* \simeq 0.87$ K. These features in $C_p(T)$ data do not appear to be a result of any conventional long-range order or spin freezing. The weak kink at T^* is systematically suppressed in an increasing magnetic field (H) up to 80 kOe. The $T^{\max}$ is somewhat stable up to 80 kOe, but it is also slightly shifted and suppressed for $H > 80$ kOe. At $H \geqslant 80$ kOe, the magnetic heat capacity C_m at low temperatures shows a power-law (T^{α}) behavior with an exponent (α) slightly less than 2. The appearance of such a nearly T^2 behavior in the $C_m(T)$ data under magnetic field infers the possible realization of a field tuned QSL behavior in $PbCuTe_2O_6$.

II. EXPERIMENTAL DETAILS

The polycrystalline samples were prepared by solid-state reaction method using high-purity PbO, CuO, and TeO_2. The stoichiometric amounts of starting materials were ground thoroughly, pelletized, and subsequently fired at 500 °C for 3 days, after sealing in an evacuated quartz tube. To get single phase of $PbCuTe_2O_6$, the sample was subjected to three intermediate grindings at the same temperature. The x-ray powder diffraction (XRD) pattern was recorded at room temperature using PANalytical X'pert PRO diffractometer. The crystal structure was refined by the Rietveld method on the powder XRD data. The magnetic susceptibility of the sample was measured on SQUID-VSM (Quantum design), in the temperature (T) range 2–300 K, under a magnetic field (H) of 10 kOe. Heat capacity C_P measurements were performed down to 0.35 K, using a PPMS with ^{3}He attachment, in fields up to 140 kOe.

III. RESULTS

A. X-ray diffraction and structural features

In order to identify the crystal structure of $PbCuTe_2O_6$, initial parameters corresponding to the choloalite mineral compound $PbCuTe_2O_6Cl_{0.33}$ [16] were used. The experimental powder diffraction pattern of $PbCuTe_2O_6$ matches well with the calculated powder pattern generated from the mineral's data, using POWDER CELL software [17]. We then refined the structure of $PbCuTe_2O_6$ by employing Rietveld refinement software [18] (see Fig. 1). The refined atomic coordinates are summarized in Table I, and the lattice constant was found to be $a \simeq 12.49 \pm 0.005$ Å. The residual factors are found to be $R_p \simeq 3.099\%$, $R_{\rm wp} \simeq 4.279\%$, $R_{\rm exp} \simeq 2.024\%$, $R_{\rm Bragg} \simeq 1.916\%$, and goodness of fit (GOF) $\simeq 2.113$, respectively. To verify the quality of our fit done by Rietveld refinement method, we also used Le Bail method [19], which is a simple method to extract the integrated intensities for powder diffraction pattern using only space group, lattice constants, profile, and back ground parameters. Structural parameters are not used in the refinement cycles. Using the same space group ($P4_132$), it provided a reasonably good fit to the experimentally observed data with a GOF about 3.213 and the obtained residual factors are also nearly consistent with the Rietveld refinement.

The structure of $PbCuTe_2O_6$ consists of CuO_4 square plaquettes, TeO_3 units, and Pb atoms, as shown in Fig. 2(a).

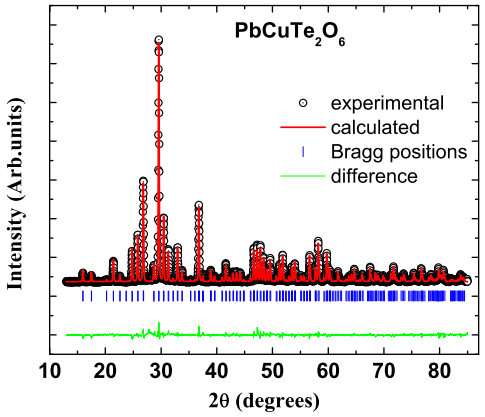

FIG. 1. (Color online) The Rietveld refinement for the powder x-ray diffraction of $PbCuTe_2O_6$. The open circles indicate the observed data, while the Rietveld refinement fit is shown as a red solid line. The Bragg positions and the difference curve are denoted by vertical blue dashes and green line, respectively. The residual parameters for the Rietveld refinement are $R_p \simeq 3.099\%$, $R_{\rm wp} \simeq 4.279\%$, $R_{\rm exp} \simeq 2.024\%$, $R_{\rm Bragg} \simeq 1.916\%$, and goodness of fit (GOF) $\simeq 2.113$, respectively.

As shown in Fig. 2(b), the arrangement of Cu atoms in this structure suggests it to be a 3D network of corner-shared triangles ($z = 6$) with a combination of first nearest-neighbor (nn) and second nn interactions. The first nn distance between Cu atoms in each CuO_4 plaquette is about (4.37±0.002) Å and an exchange coupling might be possible via O-Pb-O linkages with a bond angle 91.3° [see Fig. 2(c)]. Taking this bond length (4.37 ± 0.002) Å into consideration, the Cu atoms appear to form isolated triangles in the structure, as can also be seen in Fig. 2(c) indicated by blue triangles. Herein, we call this coupling $J_{\rm tri}$. These blue triangles are connected with each other via other equilateral triangles of side (5.60 ± 0.002) Å. Like $J_{\rm tri}$ (first nn), this second nn path is clearly mediated by TeO_3 units [see Fig. 2(a)], however, it has a larger bond length than that of the first nn blue triangle. The triangles with only this bond distance 5.60 Å (red color) form a network as in a hyper-kagome lattice, i.e., corner-shared triangles with the exchange coupling $J_{\rm hyper}$ [see Fig. 2(d)]. If we consider the first nn coupling to be very weak ($J_{\rm tri} \simeq 0$), then the second nn coupling leads to the formation of a hyper-kagome lattice exactly like that of Ir sites in $Na_4Ir_3O_8$ (which has $z = 4$). But in reality, $J_{\rm tri}$ might not be negligible so $PbCuTe_2O_6$ has a higher connectivity than that of the hyper-kagome lattice. In addition to the first nn and second nn couplings, we also

TABLE I. Unit cell parameters of $PbCuTe_2O_6$ [space group $P4_132$ (No. 213) with the lattice constant $a = 12.49 \pm 0.005$ Å].

atom	Wyckoff position	x	y	z	occ.
Te	24e	0.0812	0.4406	0.3401	1
Pb1	8c	0.1918	0.1918	0.1918	1
Pb2	4a	0.375	0.375	0.375	1
Cu	12d	0.125	0.2321	0.4821	1
O1	24e	0.0331	0.1205	0.2774	1
O2	24e	0.1771	0.3164	0.3812	1
O3	24e	0.1902	0.5240	0.2631	1

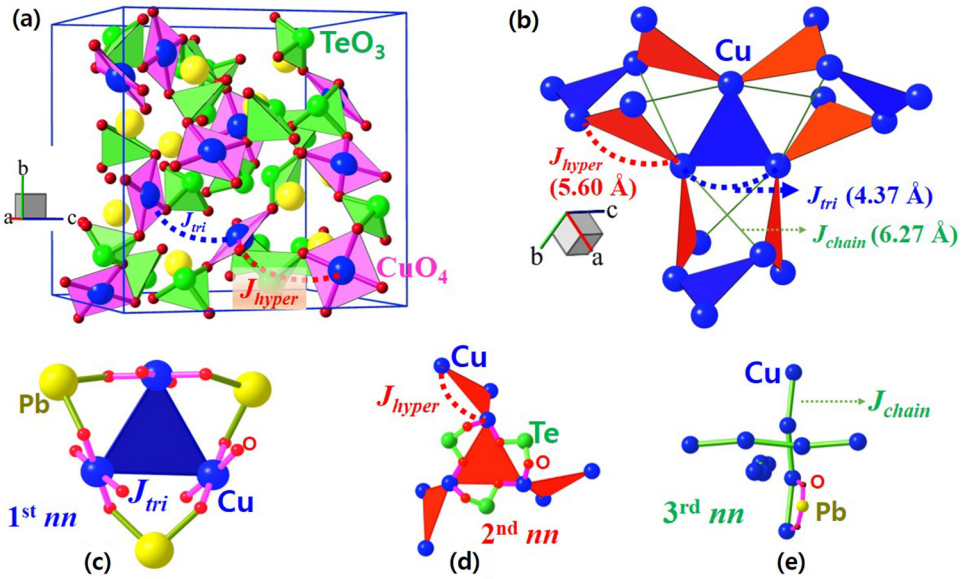

FIG. 2. (Color online) (a) The crystal structure of $PbCuTe_2O_6$. (b) The Cu network is built up of corner-shared triangles of two kinds (blue and red) with different Cu-Cu bond lengths 4.37 and 5.60 Å, respectively. (c) Formation of triangles (blue) by the first *nn* between Cu atoms with a bond length of 4.37 Å. (d) A hyper-kagome network (with red triangles) is formed when only the second *nn* between the Cu atoms of the bond length 5.60 Å are considered. (e) The third *nn* bond makes the uniform chains, which pass along all three crystallographic directions.

looked at the third *nn*, which leads to the formation of uniform chains with a bond length of 6.27 Å. These uniform chains run along all the crystallographic axes [see Fig. 2(e)]. As the bond length is large, this chain coupling (J_{chain}) is expected to be weaker than J_{hyper}.

B. $\chi(T)$ and $C_p(T)$ results

The magnetic susceptibility $\chi(T)$ [$= M(T)/H$] is measured in the temperature (T) range 2–300 K in an applied field (H) of 10 kOe, as illustrated in Fig. 3(a). The data follow a Curie-Weiss behavior and no long-range order (LRO) is detected. The absence of ZFC and FC bifurcation in thermal hysteresis measurements done with 100 Oe down to 2 K [see inset of Fig. 3(a)], indicates the absence of spin glass and/or freezing behavior. From a fit of the $\chi(T)$ data to $\chi_\circ + \frac{C}{T-\theta_{\text{CW}}}$ in the T range from 20 to 300 K, we get $\chi_\circ \simeq -(1.2 \pm 0.05) \times 10^{-4}$ cm^3/mol Cu, $C = Ng^2\mu_B^2 S(S+1)/3k_B \simeq (0.38 \pm 0.05)$ cm^3 K/mol Cu, and $\theta_{\text{CW}} \simeq -(22 \pm 0.5)$ K. Here, N_A, g, μ_B, k_B, and θ_{CW} are the Avogadro number, Lande-g factor, the Bohr magneton, the Boltzmann constant, and the Curie-Weiss constant, respectively. The core diamagnetic susceptibility (χ_{dia}) of $PbCuTe_2O_6$ was calculated to be -1.65×10^{-4} cm^3/mol formula unit from those of its ions [Pb^{2+}, Cu^{2+}, and $(TeO_3)^{2-}$] [20]. The estimated Van-Vleck paramagnetic susceptibility $\chi_{vv}(=\chi_0 - \chi_{\text{core}})$ is found to be $\simeq 4.5 \times 10^{-5}$ cm^3/mol, which is in good agreement with that in the other cuprates [21]. A negative θ_{CW} value suggests that spin correlations are antiferromagnetic in nature. The estimated effective moment (μ_{eff}) of Cu^{2+} is 1.73 μ_B, same as the $S = 1/2$ value.

In order to gain further insights into the ground state of the system, the heat capacity (C_p) measurements were performed down to 350 mK in magnetic fields up to 140 kOe. To extract the associated magnetic heat capacity contribution C_m in the absence of a suitable nonmagnetic analog of $PbCuTe_2O_6$, the lattice part was estimated by fitting the raw data with an equation consisting of the linear combination of one Debye and several Einstein terms (see the equation below) [22]:

$$C_p(T) = C_D\left[9k_B\left(\frac{T}{\theta_D}\right)^3\int_0^{x_D}\frac{x^4e^x}{(e^x-1)^2}dx\right] + \sum_i C_{E_i}\left[3R\left(\frac{\theta_{E_i}}{T}\right)^2\frac{\exp\left(\frac{\theta_{E_i}}{T}\right)}{\left[\exp\left(\frac{\theta_{E_i}}{T}\right)-1\right]^2}\right].$$

Here, R is the universal gas constant, k_B is the Boltzmann constant, θ_D and θ_{E_i} are the Debye and Einstein temperatures. We were able to model lattice contribution with a combination of one Debye term and three Einstein terms, which fits the observed data in the temperature range 30–120 K, as shown in Fig. 3(b). The corresponding Debye and Einstein temperatures θ_D, θ_{E_1}, θ_{E_2}, and θ_{E_3} were found to be 92, 79, 200, and 525 K, respectively, and the associated coefficients (C_D, C_{E_1}, C_{E_2},C_{E_3}) were fixed in the ratio of 1:1:3:5, respectively (there are ten atoms in the primitive cell of $PbCuTe_2O_6$). The C_m was obtained after subtracting the estimated lattice contribution and the data are shown in the Fig. 4(a). We would like to note that we tried to fit the C_p data in various temperature ranges with a combination of Debye and Einstein terms. Whereas the inferred C_m below 3 K was found to be independent of the fitting details and hence is considered reliable, the C_m above 5 K was found to be very sensitive to the form used for the lattice heat capacity.

The lattice heat capacity was found to be extremely weak at low T and the estimated lattice contribution at 3 K is approximately 15 times smaller than the total C_p. As illustrated in the inset of Fig. 3(b), the C_p data at zero magnetic field show an upturn below 2 K and attain a broad maximum at $T^{\max} \simeq 1.15$ K. We could observe the broad maximum directly

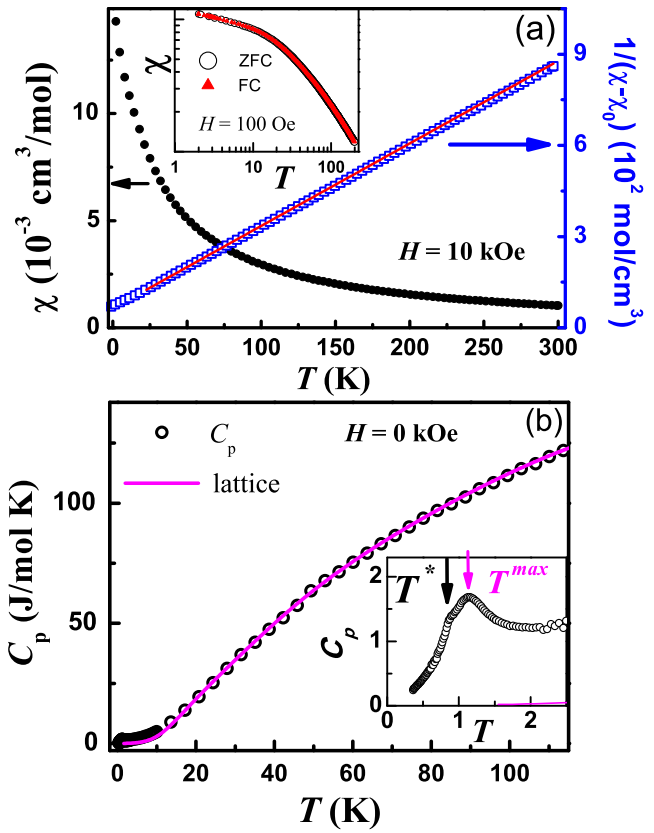

FIG. 3. (Color online) (a) The temperature dependence of the magnetic susceptibility $\chi(T)$ (left y axis) is shown. The $1/(\chi - \chi_0)$ data (right y axis) is fitted to the inverse-Curie-Weiss law. Inset shows the variation of magnetic susceptibility with temperature (note the logarithmic scale) in zero-field-cooled (ZFC) and field-cooled (FC) conditions in a magnetic field of 100 Oe. (*b*) Heat capacity C_p vs T in zero field with the fit to the lattice (solid line). Inset shows the low-T data of C_p vs T.

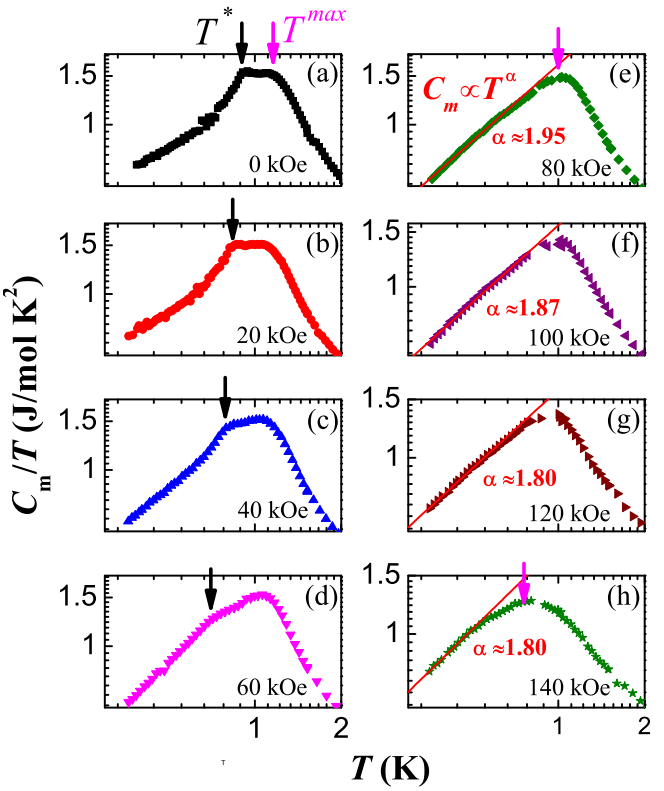

FIG. 4. (Color online) C_m/T vs T in various fields. The red line is a fit to the power law ($C_m \propto T^{\alpha}$) behavior.

in our measured C_p data due to the presence of negligible lattice contribution around that temperature. The appearance of a broad maximum has also been noticed in the plot of C_p/T versus T for many spin liquid systems [2,7,23]. This suggests that the broad maximum in our $C_p(T)$ might be a characteristic feature of highly frustrated spin systems. Generally, the position of this broad maximum in C_p data for frustrated spin systems varies according to the strength of exchange couplings, spin value and dimensionality of the system, and is found to roughly appear at $T/\theta_{\rm CW} = 0.02$ to 0.15 (see Ref. [7]). In the titled compound, we found the broad maximum at $T/\theta_{\rm CW} \simeq 0.05$, which is close to the value of 0.04 found in $Na_4Ir_3O_8$. The calculated value of $C_m\theta_{\rm CW}/T^{\rm max}$ (34 J/mol K) for $PbCuTe_2O_6$ is also similar to that of $Na_4Ir_3O_8$ indicating that the $PbCuTe_2O_6$ may have similar magnetic correlations.

Further, a weak kink is also noticed below ($T^{\rm max}$) at 0.87 K in C_p data, as marked by T^* in the inset of Fig. 3(b). This anomaly at T^* is also clearly visible as a small hump in C_m/T versus T curve in Fig. 4(a). The origin for the occurrence of this kink is not clear at this point. However, it does not seem to be a standard LRO because of the following reasons: (i) this weak kink is not a λ-like anomaly and (ii) the data well below the kink do not follow exactly a T^3 behavior (antiferromagnetic magnon dispersion). The absence of LRO down to 350 mK with a relatively large $\theta_{\rm CW}$ of −22 K and the appearance of a broad maximum at 1.15 K in C_p data all together provide a hunch of possible quantum spin liquid (QSL) ground state.

C. $C_m(T)$ in magnetic fields

The plot of magnetic heat capacity C_m divided by T (C_m/T) as a function of T in magnetic fields up to 140 kOe is shown in Fig. 4. As it is seen in the Fig. 4, the $T^{\rm max}$ is stable upto 80 kOe and it is slightly suppressed for fields $H \geqslant 80$ kOe. On the other hand, the weak kink at T^* is suppressed completely by a magnetic field of 80 kOe. The observed T^* and $T^{\rm max}$ (chosen from the plots of C_m/T versus T and C_m/T^2 versus T) are plotted in Fig. 5.

To explore the nature of excitations at low T, we fit the C_m data with a power-law ($C_m \propto T^{\alpha}$). As it is evident from the Fig. 4(a), the zero field C_m/T data do not follow a single power law below the $T^{\rm max}$ due to the presence of T^*. Upon increasing the magnetic field, the T^* is systematically suppressed and is apparently reduced to zero by magnetic fields greater than 80 kOe. Moreover, the C_m/T data seem to follow a single power law behavior for $H \geqslant 80$ kOe. We then fitted the data with a single slope (T^{α}) behavior in the temperature range 0.35–0.6 K below $T^{\rm max}$ [see Figs. 4(e)–4(h)]. The obtained values of α are near to 1.9 ± 0.1, slightly less than 2. The appearance of a near T^2 behavior in C_m data has been observed for other reported 3D QSL systems $Na_4Ir_3O_8$ and cubic-$Ba_3NiSb_2O_9$ [7,23]. In case of $Na_4Ir_3O_8$, the value of α

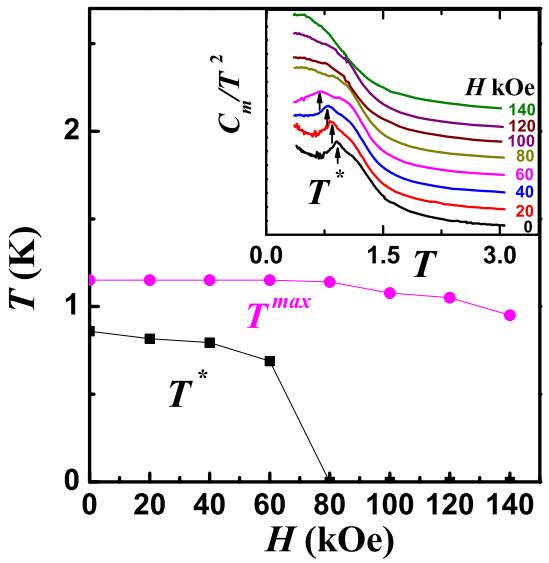

FIG. 5. (Color online) The variation of T^* and $T^{\max}$ with the applied magnetic fields. Inset shows the plot of C_m/T^2 vs T. The black arrow marks indicate the positions of T^*. Note that the data in the inset is shifted along the y axis for clarity.

is found to be in between 2 and 3, while for cubic-$Ba_3NiSb_2O_9$ the observed α value was 2.0 ± 0.2. On the other hand, in our case, the observed α value deviates slightly compared to the above examples. The reason might be due to having a different 3D frustrated spin structure for $PbCuTe_2O_6$. Several theories also predict that the T^2 dependency of the magnetic heat capacity is expected for the 3D QSLs [9]. We note that the variation of α or C_m in $PbCuTe_2O_6$ at higher magnetic fields is apparently due to the comparable strengths of Zeeman energies and the superexchange couplings in this system.

D. First-principles electronic structure calculations

In order to understand the electronic structure of $PbCuTe_2O_6$ and to identify the dominant exchange paths, we have performed first-principles density functional theory (DFT) calculations within the local density approximation (LDA) using the projector augmented-wave (PAW) method [24,25] encoded in the Vienna *ab initio* simulation package (VASP) [26,27]. The energy cutoff for the plane-wave expansion of the PAW's was taken to be 550 eV and a $(8 \times 8 \times 8)$ k mesh has been used for self-consistency. The non-spin-polarized band structure for $PbCuTe_2O_6$ is displayed in Fig. 6. The bands are plotted along the various high symmetry points of the Brillouin zone corresponding to the cubic lattice. All the energies are measured with respect to the Fermi level of the compound. The characteristic feature of the non-spin-polarized band structure, displayed in Fig. 6(a), is the isolated manifold of twelve bands near the Fermi level (E_F). These bands are predominantly of Cu $d_{x^2-y^2}$ character in the local frame of reference, arising from twelve Cu atoms in the unit cell, where Cu is at the square planar environment of O ions. The crystal-field splitting corresponding to a square planar environment is shown in the inset of Fig. 6(a). Since Cu is in 2+ state, i.e., in the d^9 configuration, these isolated bands are half-filled and are separated from the other Cu d bands by

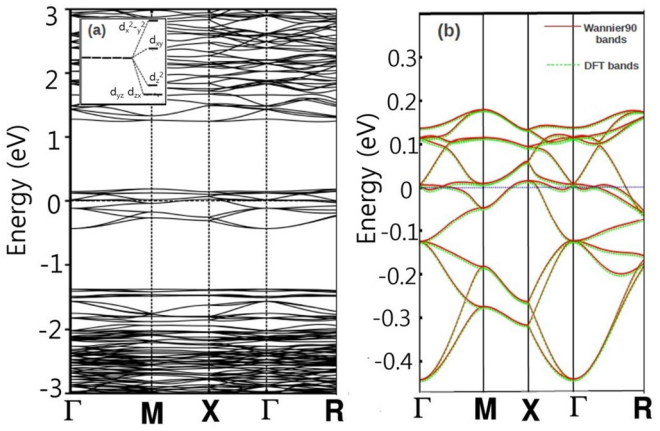

FIG. 6. (Color online) (a) Non-spin-polarised band dispersion along various high-symmetry directions. Inset shows the crystal-field splitting corresponding to the square planar environment. (b) Wannier interpolated bands superimposed on the DFT bands.

a gap of 0.9 eV. These set of twelve bands are responsible for the low-energy physics of the material.

To extract a low-energy model Hamiltonian, we have constructed the Wannier functions for these bands using the VASP2WANNIER and the WANNIER90 codes [28]. The Wannier-interpolated bands along with the LDA bands are displayed in Fig. 6(b) and the agreement is quite remarkable. The various hopping interactions (t_n) obtained in this method are listed in Table II. The superexchange interactions between the Cu atoms can be estimated using the relation $J = \frac{4t_n^2}{U_{\text{eff}}}$, where U_{eff} is the effective onsite Coulomb interaction and t_n corresponds to the hopping via superexchange paths. The relative exchange couplings are also displayed in Table II. From Table II, the J_{hyper} is found to be the strongest interaction in the system, while the J_{tri} and J_{chain} are also substantial. In order to understand why J_{hyper} is the most significant interaction and what are the superexchange paths, we look at the interesting crystal geometry of this system in Fig. 2. The second *nn* Cu atoms interact via Cu-O-Te-O-Cu path as shown in Fig. 2(d). A strong hybridization exists between the Cu $d_{x^2-y^2}$ with O p_x and O p_y orbitals via σ bonding and also with cation Te^{4+} $(5s^2)$. Moreover, this coupling involves shorter Te-O bonds (2.01 Å), whereas other couplings, J_{tri} and J_{chain}, involve a large Pb-O bond distance 2.58 Å. As a consequence, the t_2 hopping becomes most significant and gives rise to a hyper-kagome network with the coupling J_{hyper}. This is also corroborated by a plot of the Wannier function for the Cu $d_{x^2-y^2}$ orbital (see Fig. 7). The plot of Wannier function illustrates the importance of Te atoms in the exchange path J_{hyper} and it also

TABLE II. The details of bond length, hopping integrals, and the relative exchange couplings between the Cu atoms.

t_i	J_i	Cu-Cu distance (Å)	Hopping parameters (meV)	$\frac{J_i}{J_{\text{hyper}}} = \left(\frac{t_i}{t_2}\right)^2$
t_1	J_{tri}	4.37	45.59	0.54
t_2	J_{hyper}	5.60	62.18	1.00
t_3	J_{chain}	6.27	54.47	0.77

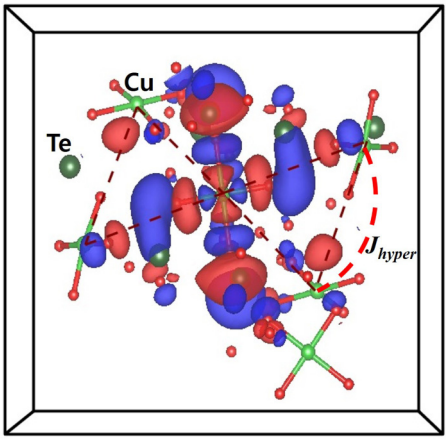

FIG. 7. (Color online) Effective Cu $d_{x^2-y^2}$ Wannier function plot.

reveals that Cu $d_{x^2-y^2}$ orbital forms strong $pd\sigma$ antibonding with the neighboring O p_x and O p_y orbitals. From the tail of the Wannier function, we find that the Te also hybridizes strongly with Cu d and O p orbitals and this hybridization is responsible for the strong second nn interaction between the Cu atoms. The next dominant interaction is the one between the third nn Cu atoms (J_{chain}). As can be seen in Fig. 1(e), the Cu atoms follow the path Cu-O-Pb-O-Cu and thereby form a 1D chain, which is actually a nonfrustrated interaction. For this coupling, the Cu $d_{x^2-y^2}$ strongly hybridizes with the O p_x orbital via σ bonding and also weakly via Pb atoms. The bond angle of O-Pb-O is 154° along this path. The third strongest exchange path is J_{tri} between the first nn Cu atoms. Here the exchange interactions between the Cu atoms follow the Cu-O-Pb-O-Cu path with a bond angle of O-Pb-O to be 92°. Due to this relatively small bond angle of O-Pb-O, the J_{tri} coupling is apparently weaker than J_{hyper}. In the light of LDA results, we can conclude that $PbCuTe_2O_6$, indeed, has a hyper-kagome network, as seen in $Na_4Ir_3O_8$, but with the considerable residual frustrated (J_{tri}) and nonfrustrated (J_{chain}) couplings, respectively.

IV. DISCUSSION

While 3D spin systems exhibit mostly ordered behavior in the absence of a special geometry, this is prevented in 1D or 2D spin systems due to the underlying strong quantum fluctuations. In some cases, the 3D spin systems can also avoid this spin-solid state and stay in the disordered and/or spin liquid ground state due to the strong frustration offered by a combined effect of geometry and the low value of spin. Such a 3D spin liquid ground state originating from strong frustration has been so far realized only in a hyper-kagome lattice $Na_4Ir_3O_8$. In this sense, $PbCuTe_2O_6$ can be a second candidate system to expect such a ground state since it has a similar space group symmetry with $Na_4Ir_3O_8$ and its spins form a corner-shared 3D frustrated network. On the other hand, the spin interaction in $PbCuTe_2O_6$ is a bit different from that of $Na_4Ir_3O_8$ in the sense that it has two comparable J_{hyper} and J_{tri} with $z = 6$ connectivity and additional nonfrustrated (J_{chain}) coupling. Even though the details are somewhat different, $PbCuTe_2O_6$ still exhibit clearly the several evidences of strong spin frustration: the absence of LRO down to 350 mK, the appearance of a broad maximum in C_p at 1.15 K, and a characteristic power-law behavior with an exponent close to 2 at low T for magnetic fields above 80 kOe. These experimental features seem to be rather similar to those observed in $Na_4Ir_3O_8$.

In contrast, the presence of a weak kink at T^* of C_p data is a distinct feature that was not observed in $Na_4Ir_3O_8$. In order to understand the true origin of T^*, here we discuss two scenarios based on the existing results in other frustrated spin systems. The first scenario is that it might be associated with a thermodynamic phase transition different from the standard LRO, with significant short-range correlations. A similar low T kink was also found in C_p/T versus T data in a polycrystalline volborthite $Cu_3V_2O_7.2H_2O$ [29]. Using ^{51}V NMR, μSR, and inelastic neutron scattering (INS) measurements, it turned out to be a kind of thermodynamic transition with dense low-energy excitations and persistent spin dynamics down to 20 mK [30]. Owing to the presence of additional nonfrustrated exchange coupling J_{chain}, $PbCuTe_2O_6$ might be also prone to have an unusual thermodynamic transition at a finite T. A similar scenario exists in $S = 1/2$, 3D frustrated double-pervoskite Ba_2YMoO_6, in which a valence-bond-glass ground state was proposed due to the involvement of the second nn coupling [31].

The second possibility is that the origin of T^* could be a signature of a valence-bond crystal (VBC), which preserves the rotational symmetry but breaks the translational invariance. Recently, Bergholtz *et al.* (Ref. [32]) have theoretically proposed a valence bond crystal (VBC) ground state for the $S = 1/2$ Heisenberg model in the hyper-kagome lattice, a contender to the other QSL proposals [9]. In their proposal, the lack of magnetic ordering as well as the existence of a peak in C_m/T have been identified as the probable tests for the VBC picture. Since our system exhibits also a weak kink in the heat capacity, this possibility might be worth consideration. On the other hand, the higher connectivity ($z = 6$) of $PbCuTe_2O_6$ than that of hyper-kagome ($z = 4$) may have to be distinguished before considering the application of the theoretical proposal. Exploring the true nature of T^* in $PbCuTe_2O_6$ is thus likely to provide an opportunity to understand the unusual ordering in highly frustrated spin networks.

V. SUMMARY

In summary, the structure of $PbCuTe_2O_6$ is made up of a 3D network with various frustrated (J_{hyper} and J_{tri}) and nonfrustrated exchange couplings (J_{chain}). The $\chi(T)$ data show relatively large AF correlations and the absence of any conventional LRO down to 350 mK. The C_m data in zero field evidence a broad maximum at $T_{\text{max}}/\theta_{\text{CW}} \simeq 0.05$ and $\frac{C_m\theta_{\text{CW}}}{T} \simeq$ 34 J/mol K, which are similar to the values found in another 3D QSL system $Na_4Ir_3O_8$. A weak kink found at 0.87 K in the C_m data is suppressed completely by a magnetic field of 80 kOe and then the C_m data follow nearly a T^2 behavior at lower temperatures. From our experimental observations, we suggest that $PbCuTe_2O_6$ might be an example of a field-induced QSL in the family of 3D frustrated Cu-based systems. To unveil more about the spin excitations of the ground state and field-induced states in detail, one needs to further explore this system intensively including NMR, μSR, and inelastic neutron scattering measurements at various energy scales.

ACKNOWLEDGMENTS

The authors B.K. and F.C.C. acknowledge the support from the National Science Council of Taiwan under project number NSC-102-2119-M-002-004. A.V.M. thanks the Department of Science and Technology, Government of India for financial support. R. Kumar and S. Bhowal acknowledge CSIR India for financial support. The work at SNU was supported by the National Creative Research Initiative (2010-0018300). We thank Fabrice Bert for fruitful discussions.

[1] C. Lacroix, P. Mendels, and F. Mila, *Introduction to Frustrated Magnetism* (Springer, Berlin, 2010).
[2] L. Balents, Nature (London) **464**, 199 (2010).
[3] J. S. Gardner, M. J. P. Gingras, and J. E. Greedan, Rev. Mod. Phys. **82**, 53 (2010).
[4] D. G. Onn, H. Meyer, and J. P. Remeika, Phys. Rev. **156**, 663 (1967).
[5] S. Hov, H. Bratsberg, and A. T. Skjeltorp, J. Magn. Magn. Mater. **15-18**, 455 (1980); P. Schiffer, A. P. Ramirez, D. A. Huse, P. L. Gammel, U. Yaron, D. J. Bishop, and A. J. Valentino, Phys. Rev. Lett. **74**, 2379 (1995).
[6] O. A. Petrenko, G. Balakrishnan, D. McK. Paul, M. Yethiraj, G. J. McIntyre, and A. S. Wills, J. Phys.: Conf. Ser. **145**, 012026 (2009); P. P. Deen, O. A. Petrenko, G. Balakrishnan, B. D. Rainford, C. Ritter, L. Capogna, H. Mutka, and T. Fennell, Phys. Rev. B **82**, 174408 (2010).
[7] Y. Okamoto, M. Nohara, H. Aruga-Katori, and H. Takagi, Phys. Rev. Lett. **99**, 137207 (2007); Yogesh Singh, Y. Tokiwa, J. Dong, and P. Gegenwart, Phys. Rev. B **88**, 220413(R) (2013).
[8] G. Chen and L. Balents, Phys. Rev. B **78**, 094403 (2008).
[9] M. J. Lawler, H.-Y. Kee, Y. B. Kim, and A. Vishwanath, Phys. Rev. Lett. **100**, 227201 (2008); Y. Zhou, P. A. Lee, T.-K. Ng, and F.-C. Zhang, *ibid.* **101**, 197201 (2008); M. J. Lawler, A. Paramekanti, Y. B. Kim, and L. Balents, *ibid.* **101**, 197202 (2008).
[10] J. S. Helton, K. Matan, M. P. Shores, E. A. Nytko, B. M. Bartlett, Y. Yoshida, Y. Takano, A. Suslov, Y. Qiu, J.-H. Chung, D. G. Nocera, and Y. S. Lee, Phys. Rev. Lett. **98**, 107204 (2007).
[11] B. Fåk *et al.*, Phys. Rev. Lett. **109**, 037208 (2012).
[12] L. Clark, J. C. Orain, F. Bert, M. A. De Vries, F. H. Aidoudi, R. E. Morris, P. Lightfoot, J. S. Lord, M. T. F. Telling, P. Bonville, J. P. Attfield, P. Mendels, and A. Harrison, Phys. Rev. Lett. **110**, 207208 (2013).
[13] Y. Shimizu, K. Miyagawa, K. Kanoda, M. Maesato, and G. Saito, Phys. Rev. Lett. **91**, 107001 (2003).
[14] H. D. Zhou, E. S. Choi, G. Li, L. Balicas, C. R. Wiebe, Y. Qiu, J. R. D. Copley, and J. S. Gardner, Phys. Rev. Lett. **106**, 147204 (2011).
[15] S. Nakatsuji, K. Kuga, K. Kimura, R. Satake, N. Katayama, E. Nishibori, H. Sawa, R. Ishii, M. Hagiwara, F. Bridges, T. U. Ito, W. Higemoto, Y. Karaki, M. Halim, A. A. Nugroho, J. A. Rodriguez-Rivera, M. A. Green, and C. Broholm, Science **336**, 559 (2012).
[16] D. W. Powell, R. G. Thomas, P. A. Williams, W. D. Birch, and I. R. Plimer, Mineral. Mag. **58**, 505 (1994).
[17] http://www.ccp14.ac.uk/tutorial/powdcell/
[18] Juan Rodruez-Carvajal, Physica B **192**, 55 (1993).
[19] A. Le Bail, H. Duroy, J. L. Fourquet, Mater. Res. Bull. **23**, 4467 (1988).
[20] P. W. Selwood, *Magnetochemistry*, 2nd ed. (Wiley-Interscience, New York, 1956), Chap. 2, p. 78.
[21] N. Motoyama, H. Eisaki, and S. Uchida, Phys. Rev. Lett. **76**, 3212 (1996); B. Koteswararao, R. Kumar, Jayita Chakraborty, Byung-Gu Jeon, A. V. Mahajan, I. Dasgupta, Kee Hoon Kim, and F. C. Chou, J. Phys. Condens. Matter **25**, 336003 (2013).
[22] Charles Kittel, *Introduction to Solid State Physics* (Wiley, Singapore, 1996).
[23] J. G. Cheng, G. Li, L. Balicas, J. S. Zhou, J. B. Goodenough, C. Xu, and H. D. Zhou, Phys. Rev. Lett. **107**, 197204 (2011).
[24] P. E. Blöhl, Phys. Rev. B **50**, 17953 (1994).
[25] G. Kresse and D. Joubert, Phys. Rev. B **59**, 1758 (1999).
[26] G. Kresse and J. Hafner, Phys. Rev. B **47**, 558 (1993).
[27] G. Kresse and J. Furthmuller, Phys. Rev. B **54**, 11169 (1996).
[28] A. A. Mostofi, J. R. Yates, Y.-S. Lee, I. Souza, D. Vanderbilt, and N. Marzari, Comput. Phys. Commun. **178**, 685 (2008).
[29] S. Yamashita, T. Moriura, Y. Nakazawa, H. Yoshida, Y. Okamoto, and Z. Hiroi, J. Phys. Soc. Jpn. **79**, 083710 (2010).
[30] A. Fukaya, Y. Fudamoto, I. M. Gat, T. Ito, M. I. Larkin, A. T. Savici, Y. J. Uemura, P. P. Kyriakou, G. M. Luke, M. T. Rovers, K. M. Kojima, A. Keren, M. Hanawa, and Z. Hiroi, Phys. Rev. Lett. **91**, 207603 (2003); F. Bert, D. Bono, P. Mendels, F. Ladieu, F. Duc, J. C. Trombe, and P. Millet, *ibid.* **95**, 087203 (2005); H. Yoshida, Y. Okamoto, T. Tayama, T. Sakakibara, M. Tokunaga, A. Matsuo, Y. Narumi, K. Kindo, M. Yoshida, M. Takigawa, and Z. Hiroi, J. Phys. Soc. Jpn. **78**, 043704 (2009); M. Yoshida, M. Takigawa, H. Yoshida, Y. Okamoto, and Z. Hiroi, Phys. Rev. Lett. **103**, 077207 (2009).
[31] M. A. de Vries, A. C. Mclaughlin, and J. W. G. Bos, Phys. Rev. Lett. **104**, 177202 (2010).
[32] E. J. Bergholtz, A. M. Laeuchli, and R. Moessner, Phys. Rev. Lett. **105**, 237202 (2010).